International Journal of Recent Technology and Engineering (IJRTE)
ISSN: 2277-3878 (Online), Volume-8 Issue-6, March 2020

Modeling and Simulation of PEM Fuel Cell Electric Vehicle with Multiple Power Sources

Ajayan S, A Immanuel Selvakumar

***Abstract*: This paper provides detailed modeling and simulation of a proton exchange membrane (PEM) fuel cell electric vehicle. The power supply system consists of a PEM fuel cell and a battery bank. The power management system effectively manages the supply flow from the dual power supply system without compromising the efficient working condition of both power supply systems. The mathematical modeling of each subsystem of the hybrid electric vehicle is presented. All the subsystems are then combined and simulated and the results are presented and discussed.**

***Keywords* : Power management system, Electric vehicle, Lithium-ion battery bank, Proton Exchange Membrane Fuel cell.**

I. INTRODUCTION

Nowadays. the automotive industry is using more electrical systems to satisfy the growing vehicular load demands. Thus, it is commanding that automobile industries will evidently undergo a drastic change within the next 5-10 years. **Error! Reference source not found.** shows world carbon dioxide emission [1][2] and it is on its rise day by day, the transportation sector being the main contributor to pollution. Currently, the demand for hybrid vehicles is increasing because of the awareness of pollution and researches is going on to develop vehicles powered by renewable energy such as wind, solar, hydraulic, etc. [3]. But because of the intermittent nature of these sources, it has become essentiality to use a storage unit such as a battery bank. Fuel cells are one of the hopeful technologies for clean electricity generation, which are very efficient when compared to internal combustion engines [4]. The fuel cells were invented back in 1839 with the innovation of the reversal of the electrolysis process. Many automotive makers have shown curiosity in hydrogen fuel cell electric vehicles. These vehicles can have more range compared to a normal electric vehicle because of the onboard power generating systems, the fuel cells [5]. They produce no carbon dioxide at all, but a small amount of carbon dioxide is produced at the time of production of hydrogen from hydrocarbons [6]. It would be zero if the hydrogen production is by renewable means like solar dissociation of water or electrolysis [7]. A normal fuel cell comprises of two electrodes parted by an electrolyte. In a fuel cell, water is formed as a result of a reaction between hydrogen and oxygen, while producing electricity. Depending on the type of electrolyte used, there are diverse fuel cells. To attain substantial voltages at output, many fuel cells have to be clubbed in series and parallel to form a stack. In utmost of the hydrogen fuel cell electric vehicles, PEM fuel cells are deployed because of the low operating temperature and fast start-up compared to other types [8]. PEMFCs can deliver power from a few kW to several hundred kW. Many automotive manufacturers including GM, Tata, Ford, Mahindra, Mercedes-Benz, Hyundai, Nissan, Volkswagen, Toyota, and Honda, introduced samples of PEM fuel cell vehicles quite a lot of years ago [9][10]. These working sample prototypes have
been evaluated on real roads, and their performance metrics have been fine-tuned so much since then. Nevertheless, the major blocking factors to fuel cell commercialization are durability and cost. By 2035, hydrogen is going to be the most favorable fuel when compared to other synthetic alternatives[11]. When fuel cell schemes are operated less in dynamic conditions and more in more steady state condition, the operating lifetime of fuel cells in fuel cell electric vehicles can be extended. Hence to meet the dynamic energy requirements, dual or multiple energy storage systems such as battery or supercapacitor or both could be used [12]. Along with meeting the accelerating power requirement, the storage systems can be used to harvest the regenerative braking power, which is not possible when using fuel cell alone. In this work, a dual power supply system consisting of PEM fuel cell and battery bank supplying power to an electric driven vehicle is discussed [8]. The power management system dictates the power flow from the two

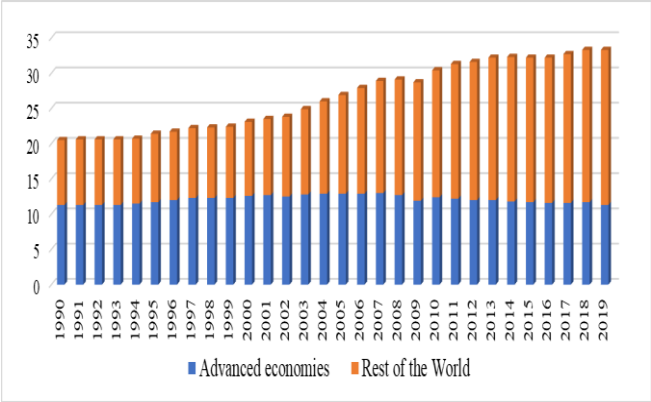

Fig. 1 Carbon dioxide emissions from 1990 to 2019

Manuscript received on February 10, 2020.
Revised Manuscript received on February 20, 2020.
Manuscript published on March 30, 2020.
* Correspondence Author
Ajayan S*, EEE Department, Karunya Institute of Technology and Sciences, Coimbatore, Tamilnadu, India. Email: ajayan85@gmail.com
A Immanuel Selvakumar, EEE Department, Karunya Institute of Technology and Sciences, Coimbatore, Tamilnadu, India. Email: immanuel@karunya .edu

sources to the traction motor as well as it manages the reverse power flow from the motor to the battery bank during regenerative braking. Here, in this case, a PMSM of 100kW is used for propulsion of the EV. A flux weakening vector control scheme is deployed to control PMSM to reach a top speed of 12500rpm. The entire system is discussed, modeled and simulated using the Simulink simulation tool. A state-machine strategy-based power management system is used for simulation of the
whole system and the obtained simulation results are showed and deliberated.

The work is structured as follows: Section II discusses an overall fuel cell vehicle system, whereas Section III presents a detailed modeling of each subsystem of the vehicle. Section IV gives an insight of the power management system and Section V details the simulation and its results followed by conclusion in Section VI.

II. FCEV SYSTEM

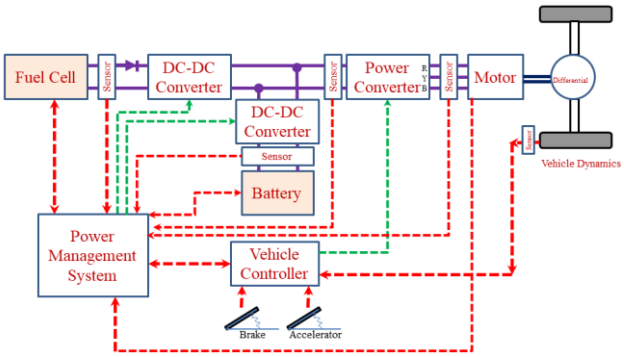

Fig. 1 FCEV System

The FCEV system essentially comprises a PEM fuel cell, two DC-DC converters [13], one DC-AC converter supplying a PMSM, a storage battery and a vehicle controller as depicted in Fig. 1. The power management system, based on state machine power strategy, operates according to different modes (Fig. 14) and relying on the power available from the dual sources. The fuel cell A unidirectional DC-DC converter is connected to PEM fuel cell as return of power is not conceivable. However, the DC-DC converter for battery and DC-AC converter for motor are bi-directional, enabling bidirectional power flow.

III. MODELING OF FCEV SYSTEM

A. PEM fuel cell model

In PEMFC, electrochemical reaction takes place consuming oxygen and hydrogen to produce water and some amount of heat [14]. During the process, chemical energy is transformed into electricity which can be utilized for powering a traction motor or stored in a battery. A PEMFC is associated with all necessary ancillaries for its operation. Depending on the type of the electrolyte present, there are various types of fuel cells out of which, PEM fuel cell being widely considered for vehicle application. A reduced model of PEMFC is ergo used for analysis and simulation in this paper. The analysis and behavior of a PEM fuel cell can be completed by an equivalent electrochemical circuit as drawn in Fig. 2.

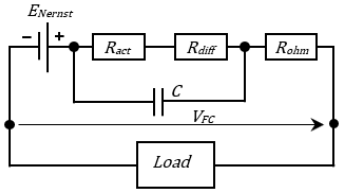

Fig. 2 Electrical equivalent circuit of PEMFC

The output voltage obtained from a single cell, according to the Nernst equation, V_{FC} can be given as[8], [14], [15]:

$$V_{FC} = E_{Nernst} - U_{act} - U_{ohm} - U_{diff} \quad (1)$$

where E_{Nernst} is the open circuit thermodynamic potential of the cell, U_{act} is the activation overvoltage, U_{diff} is the diffusion overvoltage and U_{ohm} is the resistive or ohmic overvoltage [8].

$$E_{Nernst} = 1.229 - (T_{FC} - 298.15) \times 0.85 \times 10^{-3} + T_{FC} \times 4.3085 \times 10^{-5} \times (\ln P^*_{H_2} + 0.5 \ln P^*_{O_2}) \quad (2)$$

If the output by-product water is in steam form, 1.229V should be replaced by 1.118V, T_{FC} is the temperature of the cell (Kelvin), $P^*_{O_2}$ and $P^*_{H_2}$ are the partial pressures (atm) of oxygen and hydrogen, respectively.

The fuel cell must be able to provide the power commanded by the vehicle considering its efficiency. To calculate the activation overvoltage, Tafel equation is used:

$$U_{act} = \beta_1 + \beta_2 \times T_{FC} + T_{FC} \times \beta_3 \times \ln(I_{FC}) + T_{FC} \times \beta_4 \times \ln(C^*_{O_2}) \quad (3)$$

where β_i are parametric coefficients, I_{FC} is load current of cell (A), $C^*_{O_2}$ is oxygen concentration in dissolved water film interface in the surface of catalytic cathode (mol/cm^3) and is given by

$$C^*_{O_2} = \frac{P_{O_2}}{5.08\times10^6 \times \exp^{(-498/T_{FC})}} \quad (4)$$

Resistive or ohmic overvoltage is given by [16]

$$U_{ohm} = \frac{I_{FC}}{A_{cell}} \times \left(\frac{181.6 \times \left[1 + 0.03 \times \left(\frac{T_{FC}}{A_{cell}}\right) + 0.062 \times \left(\frac{T_{FC}}{303}\right)^2 \times \left(\frac{I_{FC}}{A_{cell}}\right)^{2.5}\right]}{\left[\lambda - 0.634 - 3 \times \left(\frac{I_{FC}}{A_{cell}}\right)\right] \times \exp^{\left[4.18 \times \left(\frac{T_{FC}-303}{T_{FC}}\right)\right]}} \times l_M + A_{cell} \times R_c \right) \quad (5)$$

where, A_{cell} is membrane area (cm^2) of active cell, l_M is the membrane thickness (cm), R_c represents electrode contact resistance for proton conduction (Ω) and λ is an adjustable parameter. The denominator exponential term is the temperature factor correction for a cell temperature other than 30^{0}C.

Because of flow resistance, the input gases cannot be distributed resulting in diffusion or concentration overvoltage and is given by,

$$U_{diff} = -\ln\left(1 - \frac{J_{FC}}{J_{FC_{max}}}\right) \times B \quad (6)$$

where $J_{FC_{max}}$ is the maximum value of current density (A/cm^2) and B is cell type-dependent parameter.

Normally a number of cells are connected to get the required output and for a fuel cell containing n quantity of cells, the voltage is given by

$$V_{Stack} = n \times V_{FC} \quad (7)$$

In a PEM fuel cell, a solid membrane separates the two electrodes acts as a dielectric in a double charged layer or it can be considered as a capacitor. This effect also has to be considered while modeling and therefore, the dynamic model of the PEM fuel cell is described by [16]:

$$\frac{dv_d}{dt} = \frac{1}{C} \times I_{FC} - \frac{1}{\tau} \times v_d \quad (8)$$

where C represents the equivalent capacitance associated with U_{act} and U_{diff}, v_d represents the dynamic voltage across the capacitor equivalent (Fig. 2) and τ is electrical time constant of the fuel cell (a function of time) and is given by [16].

$$\tau = C \times (R_{act} + R_{diff}) = C \times \left(\frac{U_{act}+U_{diff}}{I_{FC}}\right) \quad (9)$$

Rewriting (1) we have

$$V_{FC} = E_{Nernst} - v_d - (I_{FC} \times R_{ohm}) \quad (10)$$

PEM fuel cell dynamic model of in Simulink is as depicted in Fig. 3.

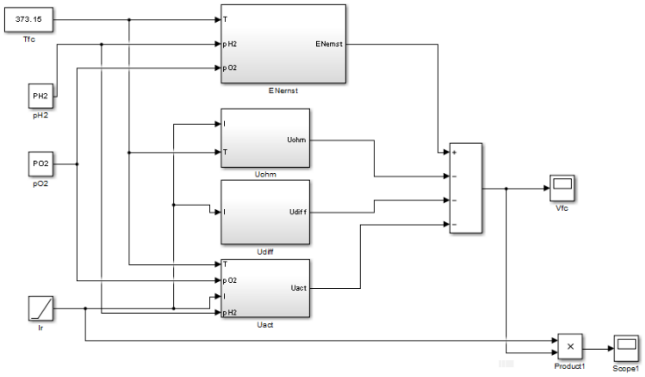

Fig. 3 Simulink diagram of PEM fuel cell

The voltage-current density characteristics give information on the operation of the fuel cell and is given in Fig. 4.

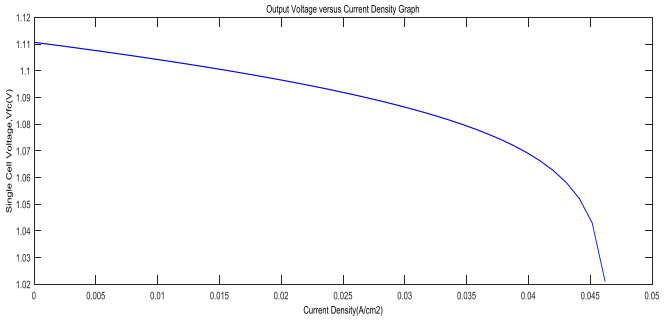

Fig. 4 Voltage versus current density characteristics of a single FC

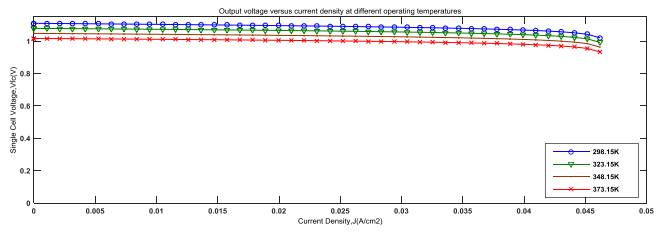

Fig. 5 Temperature dependence characteristics

From the results obtained, it can be concluded that the temperature proportionately affects the fuel cell power output.

B. Battery Bank

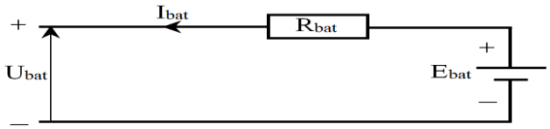

Fig. 6 Equivalent circuit of a battery

A battery model as one given in Fig. 6 is deployed in this work. Out of the many test and proven battery systems in electric and hybrid vehicles such as Lead-Acid, Ni-MH, Ni-Cd or Li-ion batteries, Lead-Acid battery is commonly used in electric cars as it is cheap, but the disadvantage is that it has deprived charge/discharge capacity. The performance of Li-ion is better than a Lead-Acid battery, and moreover, Li-ion batteries are much lighter than other types [17]. This makes it a suitable candidate for electric vehicles as it increases the range of the vehicle because of its lower weight. Li-ion battery is modeled by using the equations (11) to (14) and the Simulink model is as framed in Fig. 7.

The expression for battery voltage can be given as [18][19].

$$U_{bat} = E_{bat} - R_{bat} I_{bat} \quad (11)$$

where: U_{bat} is the battery voltage, E_{bat} is the internal emf, I_{bat} is the current flowing through battery and R_{bat} is the battery internal resistance.

The no-load voltage of the battery, whether it is in charging or discharging condition, depends on its extracted capacity, current hysteresis phenomenon during the charge and discharge cycles. It can be calculated as [18]:

During discharge(i*>0), the battery model is given as:

$$E_{bat\,disc} = E_0 - K.\frac{Q}{Q-i_t}.i^* - K.\frac{Q}{Q-i_t}.i_t - A.e^{(-B.i_t)} \quad (12)$$

And during the charge (i* <0):

$$E_{bat\,char} = E_0 - K.\frac{Q}{|i_t|+0.1\,Q}.i^* - K.\frac{Q}{Q-i_t}.i_t - A.e^{(-B.i_t)} \quad (13)$$

Where E_0 is the constant voltage, i^* is the low-frequency current dynamics(A), K is the polarization constant (A/h), i is current in the battery (A), i_t is the extracted capacity (Ah), Q is the battery maximum capacity (Ah), A is exponential voltage (V) and B is exponential capacity (A/h). The hysteresis phenomenon of the battery is represented by last term in (12) and (13), during the charge and discharge cycles respectively.

The SOC of battery is estimated as [18]:

$$SOC(\%) = 100 \times \left(1 - \frac{\int i.dt}{Q}\right) \quad (14)$$

Based on the above equations, the Li-ion battery model is depicted in Fig. 7.

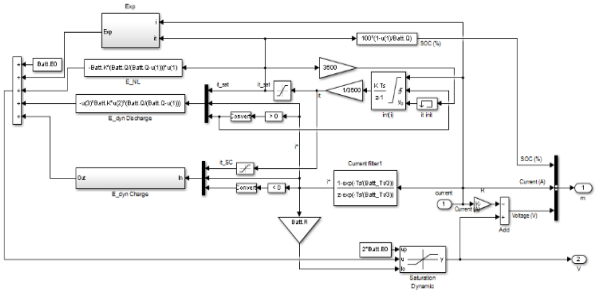

Fig. 7 Simulink model of battery.

The discharge characteristic of the battery is as plotted in Fig. 8. When battery is discharged, the first upper section in Fig. 8(a) shows the exponential voltage drop. The nominal area in Fig. 8(a) represents the charging that can be removed from the battery until the voltage falls below the nominal voltage of the battery. Finally, the rapid falling voltage section in Fig. 8(a) represents full battery discharge. Fig. 8(b) shows a discharge curve when a current of 120A is drawn from the battery.

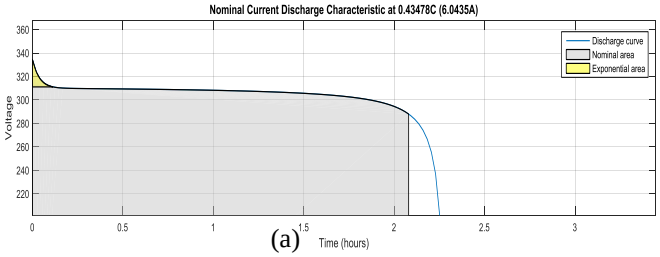

(a)

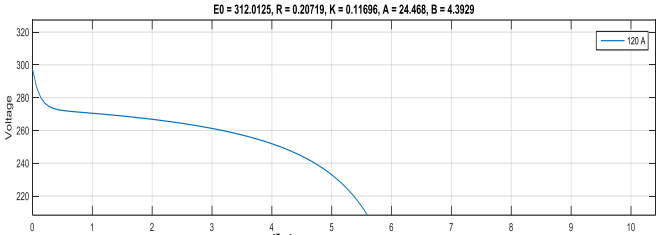

(b)

Fig. 8 Discharge curve of battery

C. Permanent Magnet Synchronous Motor description

The most popular motor technology for electric vehicle applications is Permanent magnet synchronous machines (PMSM). Many vehicles like Toyota Prius, Honda Insight and Honda FCX Clarity are fitted out with this motor. A relatively low power PMSM can drive a medium-sized car. There are many methods for speed control of PMSM out of which Field control method is widely used.

The mathematical modeling of a 3-phase two-pole PMSM is discussed. The voltage in the dq domain is expressed as follows [20]:

$$\overrightarrow{u_{dq0s}} = R_s \overrightarrow{i_{dq0s}} + p\overrightarrow{\lambda_{dq0s}} \quad (15)$$

where p is the differentiating operator d/dt, the indexes d, q , 0 and s refers to direct axis, quadrature axis, zero component of the variables and stator respectively. In the dq frame, the flux relation can be framed as follows:

$$\overrightarrow{\lambda_{dq0s}} = L_{dq0} \overrightarrow{i_{dq0s}} + p\overrightarrow{\lambda_{dq0,m}} \quad (16)$$

where the L_{dq0} (inductance matrix) is given as:

$$L_{dq0} = \begin{bmatrix} L_d & 0 & 0 \\ 0 & L_q & 0 \\ 0 & 0 & L_0 \end{bmatrix} = \begin{bmatrix} L_s & 0 & 0 \\ 0 & L_s & 0 \\ 0 & 0 & L_0 \end{bmatrix} \quad (17)$$

If the stator windings are star connected and as far as supplied with balanced 3-phase currents, then the zero-axis components can be neglected. The d and q voltage equations are:

$$u_{ds} = R_s i_{ds} + L_s \frac{di_{ds}}{dt} - \omega_r L_s i_{qs} \quad (18)$$

$$u_{qs} = R_s i_{qs} + L_s \frac{di_{qs}}{dt} + \omega_r \left(L_s i_{ds} + \lambda_{pm}\right) \quad (19)$$

Where $R_s$is the resistance of stator, L_s is the inductance of stator, ω_r the angular speed and λ_{pm} the flux of permanent magnet.

The machine's electromagnetic torque (in dq reference frame) can be expressed as defined by[20]:

$$T_e = \left(\frac{3}{2}\right)\left(\frac{P}{2}\right)\left(\lambda_{ds} i_{qs} - \lambda_{qs} i_{ds}\right) \quad (20)$$

In this simulation, an 8 pole PMSM of 288 Vdc, 100 kW rating is used. The motor specification used for simulation is given in the appendix (Table 4). The maximum motor speed that can be achieved by flux weakening vector control is 12,500 rpm.

D. Electric vehicle model

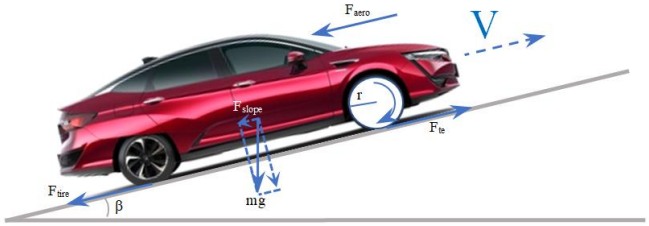

Fig. 9 Forces acting on a vehicle

The performance of the vehicle can be modeled by framing a tractive effort equation. Tractive effort is the force that propels the vehicle forward, transmitted via the drive wheels to the ground. It needs to embark on the following [21]:

Overcoming of rolling resistance;

Overcoming of aerodynamic drag;

Give the force necessary to overcome the vehicle weight portion that acts down the slope;

If the velocity is not constant, speed up or decelerate the vehicle.

Fig. 9 gives the various forces acting on a vehicle.

- Due to friction of the vehicle tires on the lane, rolling resistance force F_{tire} occurs. It is defined as:

$$F_{tire} = m \times g \times \mu_{ro} \quad (21)$$

where m is total mass of vehicle, g is gravitational constant, μ_{ro} is rolling resistance coefficient.

-Aerodynamic drag force F_{aero} caused by the dragging friction to the body of car while traveling through air. Its expression is [21]:

$$F_{aero} = \left(1/2\right) \times \rho_{air} \times A_f \times C_d \times V^2 \quad (22)$$

where ρ_{air} is density of air, V is speed of vehicle, C_d is the coefficient of aerodynamic drag and A_f is the vehicle frontal surface area.

-Climbing force F_{slope} which is dependent on the road slope.

$$F_{slope} = m \times g \times \sin(\beta) \quad (23)$$

with: β is the slope of the road.

-The acceleration force F_{acc} is the additional force that is applied to adjust the vehicle speed.

Such force will provide the vehicle's linear acceleration (a), and is given by the well-known equation derived from second law of Newton;

$$F_{la} = m \times a \quad (24)$$

Nevertheless, for a more accurate picture of the fore needed to accelerate one must also consider rotational acceleration. This is very important as the electric motor is having high moment of inertia and higher angular speed.

The axle torque $= F_{te} \times r$, where F_{te} is the powertrain's tractive effort, and r is the radius for the tires. If T_m is the motor torque and G is the system gear ratio connecting the motor to the axle, then

$$T_m = F_{te} \times \frac{r}{G} \quad (25)$$

$$\text{And } F_{te} = T_m \times \frac{G}{r} \quad (26)$$

Also, angular speed of axle $= \frac{V}{r}$ rad/s

$$\text{And angular speed of motor } \omega = G \times \frac{V}{r} \text{ rad/s} \quad (27)$$

Similarly, angular acceleration of motor

$$\frac{d\omega}{dt} = G \times \frac{a}{r} \text{ rad/s}^2 \quad (28)$$

The acceleration torque required is

$$T_m = J \times G \times \frac{a}{r} \quad (29)$$

where J is the moment of inertia of the motor rotor.

The force on the wheels required to deliver angular acceleration ($F_{\omega a}$) can be found by combining this equation with (26),

$$F_{\omega a} = J \times \frac{G^2}{r^2} \times a \quad (30)$$

As the gear system is not 100% efficient, the above equation is redefined by incorporating gear system efficiency η_g, then

$$F_{\omega a} = J \times \frac{G^2}{\eta_g r^2} \times a \quad (31)$$

Hence acceleration force is the sum of forces needed to produce linear and rotational acceleration together.

$$F_{acc} = F_{la} + F_{\omega a} \quad (32)$$

All these forces make up the total tractive effort [21]:

$$F_{te} = F_{tire} + F_{slope} + F_{aero} + F_{\omega a} + F_{la} \quad (33)$$

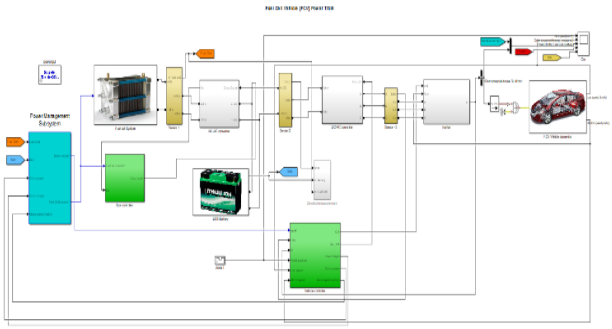

Fig. 10 Overall simulation model of FCEV in Simulink

IV. POWER MANAGEMENT SYSTEM

Power management system (PMS) should be capable of extracting different power from two sources, the battery and the fuel cell, without affecting the power delivery to the load, while maintaining the regulated output voltage of 288V. Therefore, in FCEV power management system plays an important role and needs a suitable control algorithm to handle the power flow from various sources to the load. The PMS provides reference signals to the fuel cell, motor and DC/DC converter based on the accelerator pedal position, ranging between -100% and 100% [22]. The PMS, as shown in Fig. 11, has the input parameters as drive torques, drive power, motor speed, fuel cell power, and battery voltage and SOC. Motor torque reference and FC current reference are the output parameters. The subsystem of PMS is shown in Fig. 12.

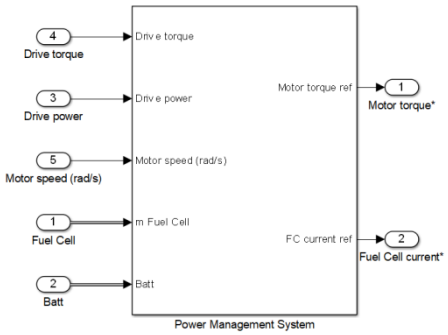

Fig. 11 Power Management System

The battery management system (Fig. 13) for Li-ion battery monitors whether the SOC is maintained within 40-80% to ensure its long life and efficiency. The complexity of PMS depends on the number and type of energy sources, as different energy sources possess distinct V-I characteristics. In addition, each source demands proper attention for their use in FCEV, as each source's dynamic and stable performance is different, as are the power and energy handling capacities.

The electric vehicle's load-power demand, powered by two sources (fuel cell and batteries), is provided as[8]:

$$P_{ld} = P_{Bat} + P_{FC} \quad (34)$$

where P_{Bat} is the battery power, and P_{FC} is the fuel cell source power.

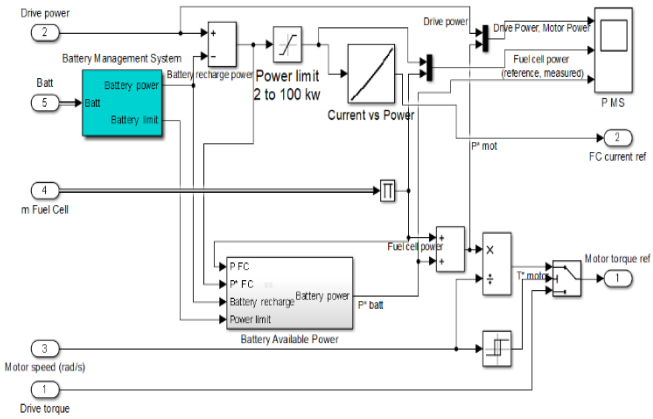

Fig. 12 PMS Subsystem

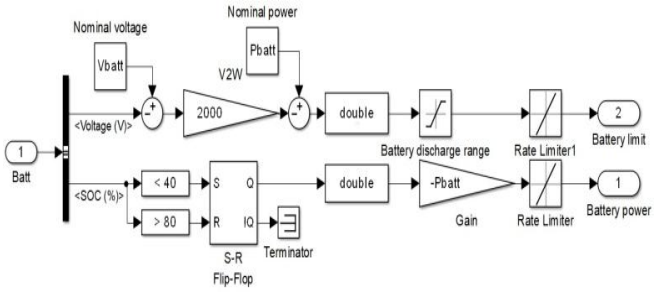

Fig. 13 BMS Subsystem

The difference of the load power demand needed by the electric vehicle is given by

$$\Delta P_{ld} = P_{ld\_new} - P_{ld\_old} \quad (35)$$

Based on the running conditions, there can be four important operating processes as shown in Fig. 14.

Acceleration mode,
Cruising mode,
Braking mode and
Standstill mode.

The two energy sources, FC and battery, must be able to cope with the power ascribed to driving (acceleration and braking) and losses in all modes, either individually or together. The different modes of the FCEV can be summarized as given in Table. 1.

Table. 1 Different modes of FCEV operation

Mode	State of Power	Description
Mode 1 Acceleration	$P_{FC}=0$ $P_{Bat}>0$ $P_{PMSM}>0$	Batteries only supply the traction motor.
	$P_{FC}>0$ $P_{Bat}=0$ $P_{PMSM}>0$	Fuel cell only supplies the traction motor.
	$P_{FC}>0$ $P_{Bat}>0$ $P_{PMSM}>0$	Fuel cell and batteries together supply the traction motor.
	$P_{FC}>0$ $P_{Bat}<0$ $P_{PMSM}>0$	Fuel cell supplies the traction motor and recharges batteries.
Mode 2 Cruising	$P_{FC}>0$ $P_{Bat}>0$ $P_{PMSM}>0$	Fuel cell and batteries together supply constant power to the traction motor.
	$P_{FC}>0$ $P_{Bat}<0$ $P_{PMSM}>0$	Fuel cell supplies constant power to the traction motor and recharges batteries.
Mode 3 Braking	$P_{FC}=0$ $P_{Bat}=0$ $P_{PMSM}=0$	No power flow.
	$P_{FC}=0$ $P_{Bat}<0$ $P_{PMSM}<0$	Batteries are recharged from the regenerated power. No fuel cell power.
	$P_{FC}>0$ $P_{Bat}<0$ $P_{PMSM}<0$	Batteries are recharged from the regenerated power and fuel cell power.
Mode 4 Standstill	$P_{FC}=0$ $P_{Bat}=0$ $P_{PMSM}=0$	No power flow.
	$P_{FC}>0$ $P_{Bat}<0$ $P_{PMSM}=0$	Fuel cell recharges the batteries.

Mode 1: Acceleration mode

During acceleration mode [22], power is drawn from both battery and fuel cell to the traction motor as the power requirement is large. Battery power will decrease after transient power is supplied. Initially, during start-up, most power is supplied by the battery due to the high response time of the fuel cell. Later, if the load power of the fuel cell is inferior, the battery ensures the traction motor's power supply and charges the batteries. If load power is greater than that provided by the fuel cell, the batteries provide the traction motor's power. The power management system takes care of:

- Battery load is limited between a min-max threshold according to SOC;
- Supply required power to the traction motor during various modes;
- Charging of batteries during regenerative braking mode and during running mode.

Mode 2: Cruising mode

During cruising mode, the vehicle moves in a constant velocity. Otherwise, the acceleration is zero. The fuel cell supplies most of the power supply to the traction motor and if the battery is in discharged state, it charges the battery too.

Mode 3: Braking mode

The load power during braking mode is negative. The kinetic energy from the wheels is utilized to charge the batteries. Hence, power is flows from the machine to charge the battery. The Fuel cells cannot be shut down immediately, and hence power produced by the fuel cell also used to charge the batteries when discharging and the charging level will depend on the storage element SOC. In braking mode, the fuel cell power can be reduced to zero, but it is mostly recommended to keep the fuel cell power production to a minimum where accepted efficiency can still be achieved. Limitations of braking mode are the full battery charging capacity, the maximum voltage and the level of braking.

Mode 4: Standstill mode

In standstill mode, the vehicle is at rest; hence the load power demand is zero. It may involve two cases: in one case, there is no power flow, that is, power provided by the fuel cell and battery is considered zero. In another case, the SOC of battery may be low and so the power produced by the fuel cell is used for charging the batteries without supplying the traction motor. The amount of power produced during this mode depends on the SOC of the battery.

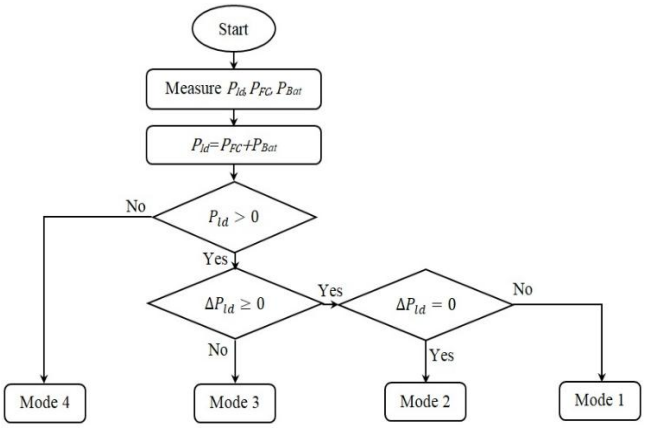

Fig. 14 Different modes of FCEV operation

V. SIMULATION RESULTS AND DISCUSSION

Combining all the modeled subsystems, an overall FCEV model is obtained as given in Fig. 10. The various subsystems are connected as per the order as depicted in Fig. 1

wherein fuel cell and battery supplies power to a common DC bus and can be controlled by their respective DC-DC converters. The accelerator pedal position is given as the input to the FCEV model, the positive value meaning acceleration and negative the deceleration (Fig. 16(a)). Based on the accelerator input, the vehicle controller provides a reference torque for PMSM and the necessary power is supplied from the DC bus. The PMS receives all the sensor inputs like fuel cell power, battery power, SOC and vehicle speed. Based on all the input parameters, the power management system manages the entire modes of operation as given by the flowchart in Fig. 14 and Table. 1. The FCEV model is simulated under Simulink and the parameters used for modeling are given in the appendix.

The voltage against current and power against current characteristics of the fuel cell stack are given in **Fig. 15**.

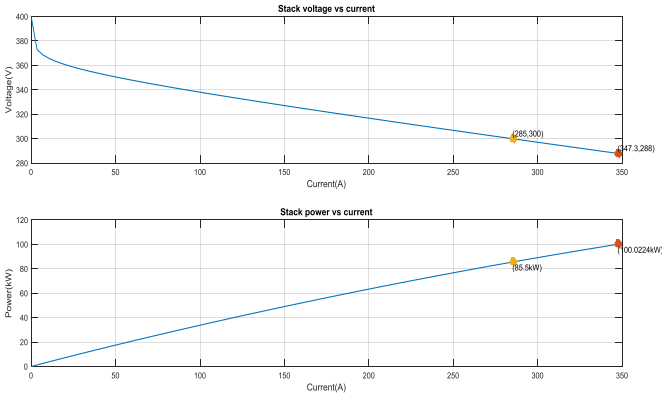

Fig. 15 Voltage against current and power against current characteristics of the fuel cell stack

Overall vehicle performance is as shown by the waveforms in Fig. 16. Initially, high acceleration is given so as to overcome the static friction and to start rolling the vehicle. The high torque requirement is met almost fully from the battery power as the response time of fuel cell is inferior to battery (Fig. 16 (d)). Once the fuel cell starts providing the power, the battery and fuel cell both share the load demand. After reaching 60 kmph, the accelerator pedal is released (8 sec to 12 sec) giving no acceleration.

In this duration, the vehicle speed decreases a little because of rolling friction and aerodynamic drag. Simultaneously, the power demand suddenly falls, and the excess power generated by the fuel cell is used to charge the battery. The

negative value of battery power in Fig. 16(d) represents charging. From 12 sec to 16 sec brakes are applied and the vehicle speed falls. This initiates regeneration of power and the battery goes into charging mode to trap maximum regenerative power. Again at 16 sec, when the vehicle accelerates, both the sources contributes for the heavy acceleration power. The power management system manages to take most of the power primarily from the fuel cell and when there is an additional requirement during acceleration, it depends on battery as well.

The performance of PMSM motor is shown in **Error! Reference source not found.**. The reference torque, shown in **Error! Reference source not found.** (a), is obtained from the vehicle controller based on the position of the accelerator pedal. As the PMSM rotor speed, given **Error! Reference source not found.** (b), varies over a wide range, it eliminates the need for an additional gear mechanism as used in normal internal combustion engine vehicles.

VI. APPLICATION FOR TRANSPORTATION

Even though installation of normal and fast charging stations is increasing, battery electric vehicle (EV) must be regularly recharged and the charging time is high [23][24]. But in fuel cell electric vehicle, there is an on-board power source and hydrogen can be filled in very quickly like normal internal combustion engine automobiles. Fuel cell alone or battery alone cannot give a better performance; hence a combination of multiple power sources can be a competitive solution. Whenever there are multiple sources for supplying power, there should be an efficient Power management control to manage and coordinate the different energy sources. In this paper, the battery bank system is used to supply energy during starting and then the power production is taken over by hydrogen fuel cell. A smooth coordination of the power sources by power management system ensures the long life of the sources and at the same time, they can be utilized at their maximum efficiency point, whatever may be the load demand. An application is made under Simulink and the simulation results shows that fuel cells has to be used with some other energy sources for getting fast response as well as to store regenerated energy during braking.

VII. CONCLUSION

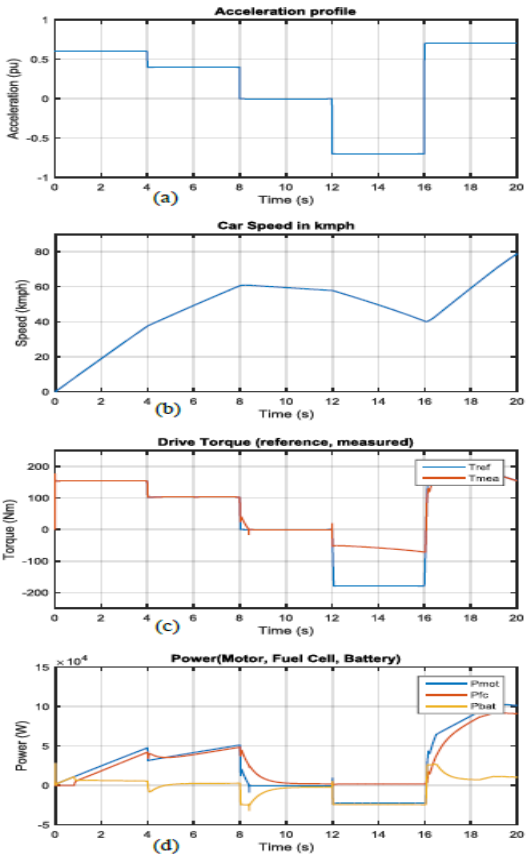

Fig. 16 Performance of vehicle: (a) Acceleration profile, (b) Car speed, (c) Drive torque and (d) Power

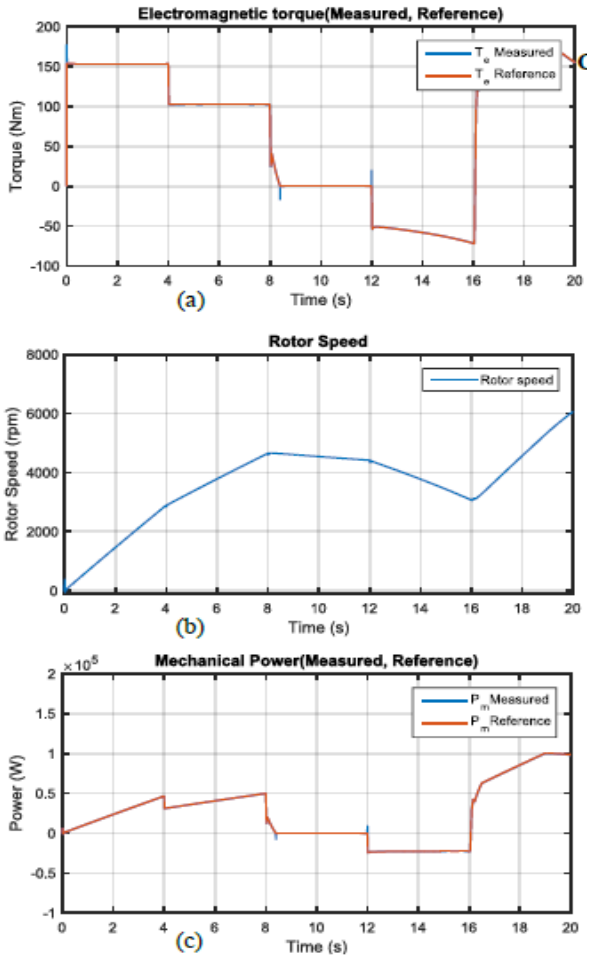

Fig. 18 Motor output characteristics: (a) Electromagnetic torque, (b) Rotor speed and (c) Mechanical power

In a nutshell, a comprehensive analysis of fuel cell electric vehicle and its components modelling depicted in this paper. The need for using multiple power sources is ascertained and a state machine strategy-based power management system with different operating modes is used for power management. The control strategy is tested in a simulation platform and different operating modes has been analyzed to check the necessity of multiple power sources to meet the traction power needed by the FCEV. Finally, the probability of the multiple source system for the production of hydrogen-powered electric vehicles enhanced by using this strategy.

VIII. APPENDIX

A1. PEM fuel cell parameters

Parameters	Values	Units
Power	100	kilowatts
Internal resistance	0.176	Ohms
Nernst voltage of single cell	1.1729	Volts
Nom. utilization-H_2	95.30	%
Nom. utilization-O_2	50.03	%
Nom. Consumption-Fuel	794.5	Std.lpm
Nom. Consumption-Air	1891	Std.lpm
Operation Temperature	370	K
Fuel cell stack size	57	litres
Air pressure	3.0	bar
Fuel cell stack weight	67.131	kg
Pressure of fuel supply	3.0	bar

A2. Vehicle parameters*

Parameters	Values	Units
Wheelbase	2.799	m
Length	4.833	m
Height	1.468	m
Width	1.846	m
Vehicle total mass	1625	kg
Rolling friction coefficient	0.02	Nm/ (rad/s)
Density of air	1.2	kg/m^3
Front area of vehicle	2.711	m^2
Tire radius	0.25	m
Aerodynamic drag coefficient	0.26	
No of wheels per axle	2	

*Honda FCX Clarity model [25][26].

A3. PMSM parameters

Parameters	Values	Units
Motor power	134	HP
Torque	256.25@ 0-3056	(Nm @ rpm)
Number of pole pairs	4	
Stator resistance R_s	0.0083	ohm
Inductance L_d	0.1742	mH
Inductance L_q	0.2926	mH
Rotor type	Salient pole (buried magnet)	
No of phases	3	

REFERENCES

1. "World carbon dioxide emissions by region 2017 | Statistic," 2018. [Online]. Available: https://www.statista.com/statistics/205966/world-carbon-dioxide-emissions-by-region/. [Accessed: 18-Nov-2019].
2. "Energy related CO2 emissions, 1990-2019 – Charts – Data & Statistics - IEA." [Online]. Available: https://www.iea.org/data-and-statistics/charts/energy-related-co2-emissions-1990-2019. [Accessed: 24-Feb-2020].
3. H. Fathabadi, "Utilizing solar and wind energy in plug-in hybrid electric vehicles," Energy Convers. Manag., vol. 156, no. December 2017, pp. 317–328, 2018.
4. O. Z. Sharaf and M. F. Orhan, "An overview of fuel cell technology: Fundamentals and applications," Renew. Sustain. Energy Rev., vol. 32, pp. 810–853, 2014.
5. C. E. Thomas, "Fuel cell and battery electric vehicles compared," Int. J. Hydrogen Energy, vol. 34, no. 15, pp. 6005–6020, 2009.
6. E. Yoo, M. Kim, and H. H. Song, "Well-to-wheel analysis of hydrogen fuel-cell electric vehicle in Korea," Int. J. Hydrogen Energy, vol. 43, no. 41, pp. 19267–19278, 2018.
7. D. Çelik and M. Yıldız, "Investigation of hydrogen production methods in accordance with green chemistry principles," Int. J. Hydrogen Energy, vol. 42, no. 36, pp. 23395–23401, 2017.
8. N. Mebarki, T. Rekioua, Z. Mokrani, D. Rekioua, and S. Bacha, "PEM fuel cell/ battery storage system supplying electric vehicle," Int. J. Hydrogen Energy, vol. 41, no. 45, pp. 20993–21005, 2016.
9. Johnson Matthey, "Fuel Cell Electric Vehicles: The Road Ahead ACKNOWLEDGEMENTS," Fuel Cell Today, vol. 3, no. July 2013, pp. 6–22, 2013.
10. T. E. Lipman, M. Elke, and J. Lidicker, "Hydrogen fuel cell electric vehicle performance and user-response assessment: Results of an extended driver study," Int. J. Hydrogen Energy, vol. 43, no. 27, pp. 12442–12454, 2018.
11. P. Runge, C. Sölch, J. Albert, P. Wasserscheid, G. Zöttl, and V. Grimm, "Economic comparison of different electric fuels for energy scenarios in 2035," Appl. Energy, vol. 233–234, no. September 2018, pp. 1078–1093, 2019.

12. D. Feroldi, M. Serra, and J. Riera, "Design and analysis of fuel-cell hybrid systems oriented to automotive applications," IEEE Trans. Veh. Technol., vol. 58, no. 9, pp. 4720–4729, 2009.
13. L. Xu, M. Ouyang, J. Li, F. Yang, L. Lu, and J. Hua, "Optimal sizing of plug-in fuel cell electric vehicles using models of vehicle performance and system cost," Appl. Energy, vol. 103, no. 2013, pp. 477–487, 2013.
14. M. Derbeli, M. Farhat, O. Barambones, and L. Sbita, "Control of PEM fuel cell power system using sliding mode and super-twisting algorithms," Int. J. Hydrogen Energy, vol. 42, no. 13, pp. 8833–8844, 2017.
15. J. P. Torreglosa, F. Jurado, P. García, and L. M. Fernández, "PEM fuel cell modeling using system identification methods for urban transportation applications," Int. J. Hydrogen Energy, vol. 36, no. 13, pp. 7628–7640, 2011.
16. N. Benchouia, A. E. Hadjadj, A. Derghal, L. Khochemane, and B. Mahmah, "Modeling and validation of fuel cell PEMFC," Rev. des Energies Renouvelables, vol. 16, pp. 2–365, 2013.
17. K. Gopalakrishnan, I. D. Campbell, M. Marinescu, M. Torchio, G. J. Offer, and D. M. Raimondo, "Optimising lithium-ion cell design for plug-in hybrid and battery electric vehicles," 15th Symp. Model. Valid. Electrochem. Energy Devices, ModVal 2018, vol. 22, no. December 2018, p. 160, 2018.
18. J. P. Torreglosa, F. Jurado, P. García, and L. M. Fernández, "Hybrid fuel cell and battery tramway control based on an equivalent consumption minimization strategy," Control Eng. Pract., vol. 19, no. 10, pp. 1182–1194, 2011.
19. Z. Wang, X. Jiao, Z. Pu, and L. Han, "Energy Recovery and Reuse Management for Fuel-electric-hydraulic Hybrid Powertrain of a Construction Vehicle," IFAC-PapersOnLine, vol. 51, no. 31, pp. 390–393, 2018.
20. D. V. Muñoz, "Design , Simulation and Implementation of a PMSM Drive System," Master Thesis, Chalmers Univ. Technol. Sweden, p. 75, 2011.
21. J. Larminie and J. Lowry, Electric Vehicle Technology Explained. Chichester, UK: John Wiley & Sons, Ltd, 2012.
22. J. J. Hwang, Y. J. Chen, and J. K. Kuo, "The study on the power management system in a fuel cell hybrid vehicle," Int. J. Hydrogen Energy, vol. 37, no. 5, pp. 4476–4489, 2012.
23. C. Will and A. Schuller, "Understanding user acceptance factors of electric vehicle smart charging," Transp. Res. Part C Emerg. Technol., vol. 71, pp. 198–214, 2016.
24. "Electric Vehicle Charging Stations Market Worth $38.9 Billion by 2027- Exclusive Report by Meticulous Research®." [Online]. Available: https://www.globenewswire.com/news-release/2020/02/17/1985723/0/en/Electric-Vehicle-Charging-Stations-Market-Worth-38-9-Billion-by-2027-Exclusive-Report-by-Meticulous-Research.html. [Accessed: 23-Feb-2020].
25. Honda Motor Co., "Honda FCX Clarity - Vehicle Specifications," Official Website, 2016. [Online]. Available: http://world.honda.com/FCXClarity/specifications/. [Accessed: 18-Nov-2019].
26. Technology Picture Book, "Honda Clarity Fuel Cell." [Online]. Available: https://global.honda/innovation/FuelCell/Clarity-Fuel-Cell-picturebook.html. [Accessed: 23-Feb-2020].

AUTHORS PROFILE

Ajayan S is currently working as Assistant professor in Department of Electrical and Electronics Engineering, Karunya Institute of Technology and Sciences, Coimbatore, Tamilnadu, India. He has 8 years of teaching experience and 3 years of industrial experience. He is pursuing his Ph.D at Karunya Institute of Technology and Sciences. His area of research includes fuel cell, electric vehicles, power electronics and drives. He is keenly doing research on naturally inspired optimization algorithms for automotive applications. He is a member of AMIE, IETE, ISTE, IAENG and SAEINDIA.

A. Immanuel Selvakumar is currently working as Professor, Department of Electrical and Electronics Engineering, Karunya Institute of Technology and Sciences, Coimbatore, Tamilnadu, India. His research has included Power System Modelling, Power System Control, Metaheuristic Optimization Algorithms, Soft Computing Techniques, Renewable Energy. He has guided many Ph.D scholars. He has published papers in various national and international journals.